HHS Public Access

Author manuscript

Cell Rep. Author manuscript; available in PMC 2018 March 05.

Published in final edited form as:

Cell Rep. 2016 July 12; 16(2): 288–294. doi:10.1016/j.celrep.2016.06.014.

2.8-Å cryo-EM structure of the large ribosomal subunit from the eukaryotic parasite *Leishmania*

Moran Shalev-Benami[1,4], **Yan Zhang**[2,4], **Donna Matzov**[1], **Yehuda Halfon**[1], **Arie Zackay**[3], **Haim Rozenberg**[1], **Ella Zimmerman**[1], **Anat Bashan**[1], **Charles L. Jaffe**[3], **Ada Yonath**[1], and **Georgios Skiniotis**[2]

[1]Department of Structural Biology, Faculty of Chemistry, Weizmann Institute of Science, Rehovot 7610001, Israel.

[2]Life Sciences Institute and Department of Biological Chemistry, University of Michigan, Ann Arbor, MI 48109, USA.

[3]Department of Microbiology and Molecular Genetics, IMRIC, Hebrew University-Hadassah Medical School, Jerusalem 9112102, Israel.

Summary

Leishmania is a single cell eukaryotic parasite of the Trypanosomatidae family, whose members cause an array of tropical diseases. The often fatal outcome of infections, lack of effective vaccines, limited selection of therapeutic drugs and emerging resistant strains, underline the need to develop strategies to combat these pathogens. The Trypanosomatid ribosome has recently been highlighted as a promising therapeutic target, due to structural features that are distinct from other eukaryotes. Here we present the 2.8-Å resolution structure of the *Leishmania donovani* large ribosomal subunit (LSU) derived from a cryo-EM map, further enabling the structural observation of eukaryotic rRNA modifications that play a significant role in ribosome assembly and function. The structure illustrates the unique fragmented nature of leishmanial LSU rRNA and highlights the irregular distribution of rRNA modifications in *Leishmania,* a characteristic with implications for anti-parasitic development.

[#]Correspondence: skinioti@umich.edu or ada.yonath@weizmann.ac.il.
[4]Co-first author.

Author Contributions

M.S.B. and A.Z. handled parasites. M.S.B purified the 91S ribosomes. Y.Z. and M.S.B. acquired cryo-EM data. Y.Z. obtained cryo-EM 3D reconstructions. M.S.B., D.M. and Y.H. built the atomic model. H.R. and M.S.B. performed the coordinate refinement of the atomic model with the help of D.M., Y.H., Y.Z. and A.B. M.S.B., Y.Z., A.Y., A.B., H.R., E.Z and G.S. interpreted the structure. A.Z. annotated and extracted the rRNA and protein sequences from the *Leishmania* strain whole genome sequence. G.S. supervised directly the EM analysis and overall project design and execution. A.Y. and A.B. supervised model building and refinement and overall project design and execution. M.S.B., Y.Z., A.B., C.L.J., A.Y. and G.S. wrote the manuscript and all authors have commented on its final version.

ACCESSION NUMBERS

The *L. donovani* LSU cryo-EM map is deposited in the Electron Microscopy Databank (EMDB) under accession code EMD-6583. The coordinates of the atomic model are also deposited in the Protein Data Bank (PDB) under accession code 3JCS.

eTOC

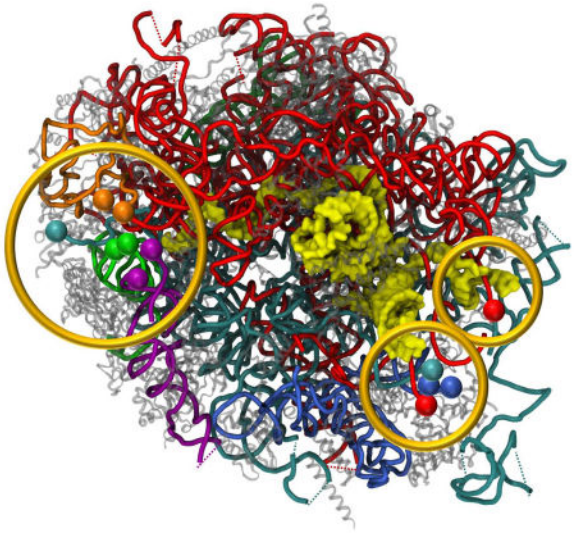

Shalev-Benami et al. describe the structure of the *Leishmania donovani* large ribosomal subunit, obtained by cryo-EM at 2.8-Å resolution. The structure shows the fragmented nature of leishmanial rRNA and highlights the irregular distribution of rRNA modifications with implications for drug development against this protozoan parasite, which afflicts millions of people worldwide.

Introduction

L. donovani belongs to a distinct order of protozoan parasites called kinetoplastids, several of which are dangerous pathogens for humans and represent a major global health concern; these include *Trypanosoma cruzi* (*T. cruzi*), *Trypanosoma brucei* (*T. brucei*) and various *Leishmania* species that cause Chagas' disease, African sleeping sickness, and leishmaniasis, respectively. Kinetoplastids are markedly diverged from other species in the eukaryotic lineage and are characterized by numerous distinct features at the genetic, biochemical and cytological levels (extensively reviewed in Fernandez-Rodrigez et al., 2014).

One particularly interesting peculiarity of kinetoplastids lies in their cytosolic ribosomes, which include an unusual segmentation of their large subunit (LSU) 26S rRNA (Hernández et al., 2014), extensive number of rRNA modification sites (Eliaz et al., 2015), and enlarged rRNA expansions (Gao et al., 2005; Hashem et al., 2013). Many studies have focused on these unique features in trypanosomatid ribosomes aiming at exploiting them as targets for the development of novel anti-parasitic drugs (Michaeli et al., 2012). Notwithstanding these efforts, the mechanism of rRNA segmentation and its biological role remain largely obscure. Cryo-EM investigations of ribosomes from *T. cruzi* and *T. brucei* at resolutions of 12 Å and 5.6 Å, respectively, have demonstrated the overall segmented architecture of kinetoplastid ribosomes (Gao et al., 2005; Hashem et al., 2013). However, the limited resolution of these earlier studies precluded the building of atomic models and understanding of functional

aspects in detail. Here we describe a high resolution structure of the large ribosomal subunit from *L. donovani* promastigotes recently isolated from a spleen biopsy of a visceral leishmaniasis patient in northern Ethiopia. The structure is based on a 2.8-Å cryo-EM reconstruction of the leishmanial LSU that enabled determination of a nearly complete atomic model. The high resolution cryo-EM map obtained in this study has also enabled the direct visualization of the unusual rRNA modification pattern in *Leishmania*. Some of these modification loci were recently predicted using bioinformatics tools (Eliaz et al., 2015), and our structure provides an experimental evidence for the existence of these modifications on the leishmanial ribosome. The *L. donovani* LSU atomic model presented here will serve as a reliable template for future structure-based drug design.

Results and Discussion

Cryo-EM analysis and model building

We employed single-particle cryo-EM to obtain a three-dimensional (3D) map of the *L. donovani* LSU at resolution of 2.8 Å. For these studies we purified intact 91S leishmanial ribosomes and initially obtained a 3D map of the entire apparatus. However, the wide range of conformations of the small subunit (SSU) relative to the LSU limited the resolution in this region. This problem was compounded by internal flexibility within the SSU, evident from our further attempts of masked refinement with signal subtraction of the LSU resulting in SSU maps with resolution lower than 4 Å (Fig. S1–S2). As such, the 3D maps for the SSU were insufficient for fully reliable model building and refinement. Thus, we focused our efforts on obtaining the structure of the 67S LSU that includes the peptide bond formation site (peptidyl transferase center; PTC), the nascent-protein exit tunnel, and several significant unique features of the leishmanial ribosome. Refinement of the LSU cryo-EM reconstruction resulted in an improved map with a global resolution of 2.8 Å. Large regions of the map, mainly located in the particle's core, showed better than 2.6-Å resolution whereas only a few highly flexible peripheral regions showed resolution lower than 3.5 Å (Fig. 1A–C, S1–3). The cryo-EM density enabled the building, refinement and validation of an atomic model with over 80% of the total rRNA content and 38 out of 43 proteins of the 67S (Fig. 2A, Table S1). Homology based models of two additional proteins with a highly flexible nature (uL6 and uL16) were docked to low resolution map areas located on the ribosome solvent exposed surface. Consistent with the reported resolution, post-transcriptional rRNA modifications such as 2'-O methylations or dihydrouridination, as well as structurally ordered solvent molecules including metal ions (Mg^{+2}) and water molecules could also be assigned in well resolved density regions (Fig. 1D–E, S3–4; Table S2). Surface exposed regions for which only partial density was visible were not included in our final model. These areas are often disordered (Ben-Shem et al., 2011; Rabl et al., 2011) and include protein uL1 that is located on the edge of the L1 stalk, an rRNA segment belonging to the GTPase center, and the L7/12 stalk along with protein uL11 and the acidic P proteins residing within the same region (Table S1). In addition, some flexible parts of kinetoplastid-specific rRNA expansion segments as well as protein eL40 could not be fully resolved and therefore their coordinates were not assigned to the final model. Mass spectroscopy (MS) analysis of the sample used for cryo-EM indicated the presence of all proteins, including the

acidic P proteins P0, and P1\P2 (Table S1), supporting our interpretation that the lack of density for these elements in our map stems primarily from their high flexibility.

Structure of the *Leishmania* ribosome LSU and comparison to other eukaryotic ribosomes

Despite the relatively low sequence conservation with other eukaryotes, the structures of leishmanial ribosomal proteins are homologous to those previously reported in high-resolution structures of yeast (Ben-Shem et al., 2011), human (Khatter et al., 2015), malaria (Wong et al., 2014) and *Tetrahymena* (Rabl et al., 2011). The main two exceptions regarding the *Leishmania* LSU protein profile are the markedly extended C-terminal of protein eL19, containing an additional ~60 residues, and the absence of protein eL41 (Table S1). eL19 and eL41 do not have counterparts in bacterial ribosomes and play an important role in the formation of the eukaryote/archaea specific inter-subunit bridges eB12 and eB14, respectively. Similar exceptions in protein composition were also highlighted in previous studies of *T. cruzi* and *T. brucei* ribosomes (Gao et al., 2005; Hashem et al., 2013) and thus do not represent unique features of the leishmanial ribosome but are likely common to all members belonging to the kinetoplastid order.

In contrast to the rather conserved ribosomal protein profile, the leishmanial rRNA content is greatly diverged from other eukaryotes, particularly in eukaryote specific expansion segments localized on the ribosome periphery (Fig. S5). Comparison of rRNA content with other trypanosomatids indicates an overall sequence similarity of 73%. Interestingly, variability is only limited to the trypanosomatid-specific rRNA expansions that highly diverge in both sequence and length. These variable expansion regions are likely to interact with satellite components that support and monitor the translational activity but are not directly involved in decoding and peptide bond formation, namely in the ribosome functional catalysis. Due to the observed variation among different species in the kinetoplastid order these regions might serve as potential selective targets for species-specific drug design.

LSU rRNA segments converge to three focal points involving 5.8S

The most striking divergence of kinetoplastid ribosomes is the atypical fragmentation of their LSU 26S rRNA into six distinct segments (Hernández et al., 2014). The 26S rRNA segments in *Leishmania* are designated as alpha (α), beta (β), gamma (γ), delta (δ), epsilon (ε) and zeta (ζ) and are composed of 1782, 1527, 213, 183, 133 and 76 nucleotides, respectively (Fig. 2B–D). These segments along with the rather conserved 5S and 5.8S rRNA fragments bring the total LSU rRNA count to eight chains, compared to only two or three chains in bacteria and other eukaryotes, respectively (Fig. 2C). Previous structures of *Trypanosoma* ribosomes at intermediate-to-low resolutions (Gao et al., 2005; Hashem et al., 2013) provided valuable insights regarding the unique rRNA fragmentation pattern in kinetoplastids. Our present cryo-EM map at 2.8-Å enabled the atomic structure of all eight rRNA chains including the delineation of specific interactions between these chains (Fig. 2B–D). The *Leishmania* ribosome LSU structure confirms that, despite the segmented nature of the rRNA, the ribosomal functional cores adopt an overall 3D architecture that is common to other eukaryotic ribosomes. In terms of sequences, the functional regions of the leishmanial ribosome are highly conserved amongst class members and are similar to other

ribosomal species. However, in contrast to most ribosomes where the functional domains are assembled from a single rRNA chain (23S/28S), the functional sites in kinetoplastid LSU are composed of three different rRNA chains. These elements are highlighted in the 2D maps derived from our 3D structure (Fig. 2D, S4), and include the PTC (beta), the peptide exit tunnel (alpha and beta), the saricin-ricin loop (SRL-loop, delta), the L1 stalk (beta) and the GTPase center (alpha). Nevertheless, despite being composed of several fragments, the structural elements are similar to other ribosomes, indicating a well-established conformational integrity that maintains the functional domains in an active state.

Strikingly, the structure shows that the ends of all rRNA fragments converge into three separate focal points, all located at solvent-exposed surface cavities (Fig. 3A). One focal point (point I) is localized in close proximity to the highly conserved LSU proteins uL3, uL13, uL22 and eL33. Focal point I includes both 5’ and 3’ ends of delta, epsilon and zeta, as well as the 5’ end of the 5.8S rRNA (Fig. 3B). Two trypanosome specific rRNA expansions, ES43L and KSE5 (Fig. S6A), also converge to this focal cavity. The second focal point (point II) includes the 3’ end of 5.8S and 5’ end of alpha chain, and maintains close interactions with the eukaryote specific protein eL8 (Fig. 3C). The third focal point (point III) is localized within a pocket defined by three eukaryote specific proteins, eL27, eL34 and eL38, and includes both ends of the gamma unit as well as alpha 3’ and beta 5’ ends (Fig. 3D). A highly flexible loop of 5.8S, which is slightly extended in trypanosomatids (ES3L, Fig. 3D), is penetrating deeply into the convergence pocket. The most notable observation resulting from this arrangement is that the 5.8S rRNA appears to be a common component of all three focal points, with three distinct domains reaching out to each of the rRNA convergence cavities. Based on this observation we hypothesize that the 5.8S rRNA might serve as an organizing center that directs rRNA folding and ribosome assembly.

Leishmanial rRNA is modified at unique positions

An additional unique property of kinetoplastid ribosomes is the unusually large number of modified rRNA positions when compared to other species (Eliaz et al., 2015; Liang et al., 2005; Michaeli et al., 2012). Earlier studies in bacteria and archaea showed the necessity of rRNA modifications for ribosomal catalytic activity and for rRNA folding during ribosome biogenesis (Green, et al., 1996; Schmeing, et al., 2005; Demirci, et al., 2010). Recent structural work on *E. coli* (Fischer et al., 2015) and *T. thermophilus* (Polikanov et al., 2015) ribosomes observed the rRNA modification pattern in bacterial ribosomes at the atomic level. These studies, which highlighted the importance of such modifications for bacterial ribosome integrity and function, demonstrated their impact on the conformation of binding pockets for several antibacterial agents. While the number of modified rRNA positions in *E. coli* and *T. thermophilus* are 35 and 23, respectively, rRNA modifications in eukaryotes usually exceed 100 modified residues (Vincent Yip et al., 2013). Despite their prevalence, the structural and functional aspects of these modifications have not yet been addressed. The majority of rRNA modifications in eukaryotes are 2’-O methylations and pseudouridinylations, with both types mediated by small nuclear RNAs (snoRNAs) that guide universal 2’-O methyltranferases and pseudouridine synthetases to the modification sites. Bioinformatics studies predicted that *Leishmania* and *Trypanosoma* ribosomes contain 165 and 142 rRNA modifications, respectively, which are mostly conserved amongst the two

species (Eliaz et al., 2015; Liang et al., 2005). Furthermore, about 40% of these modifications are predicted to be located outside the highly conserved rRNA regions that are also modified in other eukaryotes (Fig. 4A–B, S4). In the leishmanial ribosome, 99 of these modifications are predicted to occur in the LSU, with 57 2'-O methylations and 42 pseudourinylations. The methylation on 2'-O sugar could be clearly observed in our maps and we located 35 out of 57 predicted methylation sites in our structure (Fig. S4, Table S2). In addition, we observe an 11 additional methylation sites that were not predicted by the leishmanial snoRNA profile, but were previously reported in other eukaryotes (Piekna-Przybylska, et al., 2008). Even though pseudo-uridines could not be identified in density maps due to their minute chemical differences from uridines, their presence could be indirectly conferred by inspections of polar residues present in the vicinity of their N1 position (Fischer, et. al., 2015). A non-planar geometry was observed in one rRNA residue that has been predicted to be pseudo-uridinylated in *Leishmania* (U1404, chain Beta, Fig. 1E), implying that the residue has been modified to dihydrouridine rather than to a pseudouridine, as predicted.

Some rRNA modifications in bacterial ribosomes have been shown to localize in functional ribosomal targets such as the PTC, the peptide exit tunnel and the mRNA-tRNA accommodation corridor (Fischer, et al., 2015; Polikanov et al., 2015). As in prokaryotes, *Leishmania* modifications are mainly located in functional regions and are mostly present in internal ribosomal parts rather than on the periphery (Fig. 4A–B, S4). However, in trypanosomatids the number and spread of such modified residues in ribosomal functional regions is significantly increased, while we additionally observe modifications in the L1 and L7/12 stalk domains (Fig. 4A). Furthermore, trypanosomatid specific modifications are localized beyond the known functional ribosomal domains. Three 2'-O methylation sites unique to this family are localized in close proximity to the three focal points (Fig. 4B) and include two modifications on the 5.8S chain (m^2A162 and Um7 in focal points I and II, respectively) and one in alpha (Gm1628, in focal point III). The modified residues are directly involved in electrostatic interactions with residues belonging to alternate rRNA chains. Um7 and m^2A162 of 5.8S maintain base interactions with A456 and U8 of alpha, respectively, and Gm1628 of the alpha chain interacts with A18 of beta via non-canonical interactions with the sugar edge of A18 (Fig. 4C–E, S6). m^2A162 and Gm1628 also maintain electrostatic interactions with uL23, a universally conserved ribosomal protein that is involved in protein exit tunnel composition (Fig. 4D–E). Since 2'-O methylations are considered to be important for RNA stabilization, (Eliaz et al., 2015) we hypothesize that modifications in proximity to fragmented rRNA terminals may aid focal point formation during ribosome biogenesis and enhance the stability of the segmented ribosome by holding the rRNA edges intact. Ribosome stabilization might be further facilitated by close interactions between rRNA and ribosomal proteins located in the focal point vicinity (Fig. S6B–D).

Implications for kinetoplastid ribosome biogenesis

As in other eukaryotes, the rRNA in kinetoplastids is encoded as a single transcription unit that contains sequences corresponding to the 18S, 5.8S and 26S (the 5S rRNA is encoded from a separate transcription unit) (Fig. 2C). These coding regions are separated by two

internally transcribed sequences (ITS1 and ITS2) that are later processed by exo- and endo-nucleases (Woolford et al., 2013). Previous biochemical work on ribosome biogenesis in yeast and other eukaryotes indicated that the elimination of ITS1 and ITS2 from the nascent rRNA transcript is a multistep process that involves many assembly factors and the sequential incorporation of ribosomal proteins (Woolford et al., 2013; Gamalinda et al., 2014; Strunk et al., 2011). These studies demonstrated that ITS1 is cleaved very early in ribosome biogenesis, separating the 18S rRNA from the LSU components. The last cleavage step in ITS1 processing releases the 5' end of 5.8S and enables its base pairing with a complimentary sequence residing within 26S domain I to form helix 2 (H2) (Woolford et al., 2013). The cleavage of ITS2 occurs in later steps of ribosome biogenesis and results in the release of the 3' end of 5.8S from the conjugated 26S rRNA (Woolford et al., 2013). Notably, all rRNA ends composing focal point I in the leishmanial ribosome are centered in regards to the 5' end of 5.8S, whereas the rRNA ends composing focal points II and III are in close proximity to the 3' end of the 5.8S rRNA. Assuming that the processing of ITS1 and ITS2 in kinetoplastids is similar to other eukaryotes, it is possible that focal point organization during ribosome biogenesis starts with the assembly of focal point I after ITS1 cleavage, and proceeds with the assembly of focal points II and later III following the cleavage of ITS2. This order of formation of the three focal points is further supported by the relative time point of assembly of the ribosomal proteins defining the focal cavities. Analysis of yeast phenotypes resulting from mutational analysis of ribosomal proteins (Gamalinda et al., 2014) has shown that the proteins surrounding focal points I and II assemble in early steps in ribosome biogenesis, whereas proteins surrounding focal point III enter in median steps of biogenesis.

Kinetoplastid ribosome coding regions differ from those of other eukaryotes mainly in including five additional ITSs that separate the six segments of 26S rRNA. The length and sequences of these segments show significant variability between different class members, and the mechanism(s) by which they are excised from the premature ribosome are currently unknown. The observation that the rRNA segment terminals converge into three surface exposed focal points in the leishmanial ribosome (Fig. 3) strongly suggests that cleavage of these segments occurs during or post ribosome assembly, rather than in conjugation with operon transcription. In addition, given the distant location of focal point I from II and III, we hypothesize that at least two different nucleases are involved in the cleavage mechanism of the rRNA ITSs. However, it remains unclear whether the cleavage events are conjugated to focal point formation. The presence of kinetoplastid specific expansions in focal points I and III, which are unique to this class, highlights the possibility that these rRNA expansions are involved in the cleavage mechanism after or during focal point formation. It is also possible that the unique rRNA modifications around the focal points may be needed for the diverged rRNA processing events in these species. It should be noted that recent work has highlighted the role of rRNA modifications in ribosome biogenesis of other eukaryotic species (Lafontain, 2015), while earlier studies with trypanosomatids highlighted the importance of snoRNA and possibly rRNA modifications in rRNA processing (Michaeli, et al., 2012). Interestingly, our structure reveals that protein uL23 maintains close interactions with two modified rRNA residues in close proximity to focal points II and III. uL23 has been shown to be essential for rRNA processing as its absence leads to inhibition of ITS2

cleavage (Gamalinda et al., 2013), an event that is likely a key for the generation of these focal points. In any case, the *Leishmania* ribosome LSU structure illustrates the end point of ribosome maturation, and further detailed biochemical and structural investigations into intermediate species will be needed to fully decipher the mechanism of trypanosomatid ribosome biogenesis.

Conclusions

The *Leishmania* LSU structure highlights the unique nature of trypanosomatid ribosomes and the divergent pathway of their biogenesis. Understanding the mechanism of rRNA segmentation and its benefits to the translation apparatus are of great importance for the design of new therapeutic strategies that will target the parasite's ribosomes. The atomic model obtained here constitutes the structural framework for understanding events in trypanosomatid ribosome biogenesis, while also providing a solid structural basis for the development of novel and highly selective anti-parasitic agents.

Experimental Procedures

91S ribosomes were purified from *L. donovani* promastigotes by gradual centrifugation steps that included a 1.1M sucrose cushion followed by a 15–30% sucrose gradient. The samples were vitrified and data were manually recorded on a Titan Krios electron microscope (FEI) equipped with a K2 Summit direct electron detector (Gatan, Inc.). 3D reconstruction was performed using RELION 1.3 (Scheres, 2012). Model building was executed in COOT (Emsley et al., 2010) and was later refined by *phenix.real_space_refine* implemented in PHENIX (Afonine et al., 2013). See Supplemental Experimental Procedures for a detailed description of methods.

Supplementary Material

Refer to Web version on PubMed Central for supplementary material.

Acknowledgments

We thank Pavel Afonine of the Phenix development team for help and advice on model refinement, Dr. Nadav Elad for assistance with negative-stain EM screening, Dr. Yishai Levin and Dr. Meital Kupervaser for mass-spectrometry, and Dr. Moshe Peretz, Shoshana Tel-Or and Dr. Maggie Kessler for experimental support. This work was supported by the Clore Foundation for postdoctoral fellows, and the Weizmann Abroad Postdoctoral Program for Advancing Women in Science (to M.S.B), grant OPPGH5336 from the Bill and Melinda Gates Foundation (to C.L.J), and NIH R01 DK090165 (to G.S).

References

Afonine PV, Headd JJ, Terwilliger TC, Adams PD. New tool: phenix.real_space_refine. Computational Crystallography Newsletter. 2013; 4:43–44.

Ben-Shem A, Garreau de Loubresse N, Melnikov S, Jenner L, Yusupova G, Yusupov M. The structure of the eukaryotic ribosome at 3.0 Å resolution. Science. 2011; 334:1524–1529. [PubMed: 22096102]

Brown A, Shao S, Murray J, Hegde RS, Ramakrishnan V. Structural basis for stop codon recognition in eukaryotes. Nature. 2015; 524:493–496. [PubMed: 26245381]

Demirci H, Murphy F, Belardinelli R, Kelley AC, Ramakrishnan V, Gregory ST, Dahlberg AE, Jogl G. Modification of 16S ribosomal RNA by the KsgA methyltransferase restructures the 30S subunit to optimize ribosome function. RNA. 2010; 16:2319–24. [PubMed: 20962038]

Eliaz D, Doniger T, Tkacz ID, Biswas VK, Gupta SK, Kolev NG, Unger R, Ullu E, Tschudi C, Michaeli S, et al. Genome-wide analysis of small nucleolar RNAs of Leishmania major reveals a rich repertoire of RNAs involved in modification and processing of rRNA. RNA biology. 2015; 12:1222–1255. [PubMed: 25970223]

Emsley P, Lohkamp B, Scott WG, Cowtan K. Features and development of Coot. Acta. Crystallogr. D. Biol. Crystallogr. 2010; 66:486–501. [PubMed: 20383002]

Fernandez-Rodrigez JC, Godinho JL, de Souza W. Biology of human pathogenic trypanosomatids: epidemiology, lifecycle and ultrastructure. Subcell Biochem. 2014; 74:1–42. [PubMed: 24264239]

Fischer N, Neumann P, Konevega AL, Bock LV, Rodnina MV, Stark H. Structure of the *E. coli* ribosome-EF-Tu complex at <3 Å resolution by Cscorrected cryo-EM. Nature. 2015; 520:567–570. [PubMed: 25707802]

Gamalinda M, Ohmayer U, Jakovljevic J, Kumcuoglu B, Woolford J, Mbom B, Lin L, Woolford JL. A hierarchical model for assembly of eukaryotic 60S ribosomal subunit domains. Genes Dev. 2014; 28:198–210. [PubMed: 24449272]

Gao H, Ayub MJ, Levin MJ, Frank J. The structure of the 80S ribosome from Trypanosoma cruzi reveals unique rRNA components. Proc. Natl. Acad. Sci. U. S. A. 2005; 102:10206–10211. [PubMed: 16014419]

Green R, Noller HF. In vitro complementation analysis localizes 23S rRNA posttranscriptional modifications that are required for Escherichia coli 50S ribosomal subunit assembly and function. RNA. 1996; 2:1011–21. [PubMed: 8849777]

Hashem Y, des Georges A, Fu J, Buss SN, Jossinet F, Jobe A, Zhang Q, Liao HY, Grassucci RA, Bajaj C, et al. High-resolution cryo-electron microscopy structure of the Trypanosoma brucei ribosome. Nature. 2013; 494:385–389. [PubMed: 23395961]

Hernández R, Cevallos M. Ribosomal RNA gene transcription in trypanosomes. Parasitol. Res. 2014; 113:2415–2424. [PubMed: 24828347]

Khatter H, Myasnikov AG, Natchiar SK, Klaholz BP. Structure of the human 80S ribosome. Nature. 2015; 520:640–645. [PubMed: 25901680]

Lafontaine DLJ. Noncoding RNAs in eukaryotic ribosome biogenesis and function. Nat. Struct. Mol. Biol. 2015; 22:11–19. [PubMed: 25565028]

Liang XH, Uliel S, Hury A, Barth S, Doniger T, Unger R, Michaeli S. A genome-wide analysis of C/D and H/ACA-like small nucleolar RNAs in Trypanosoma brucei reveals a trypanosome-specific pattern of rRNA modification. RNA. 2005; 11:619–645. [PubMed: 15840815]

Michaeli S, Doniger T, Gupta SK, Wurtzel O, Romano M, Visnovezky D, Sorek R, Unger R, Ullu E. RNA-seq analysis of small RNPs in Trypanosoma brucei reveals a rich repertoire of non-coding RNAs. Nucleic Acids Res. 2012; 40:1282–98. [PubMed: 21976736]

Piekna-Przybylska D, Decatur WA, Fournier MJ. The 3D rRNA modification maps database: with interactive tools for ribosome analysis. Nucleic Acids Res. 2008; 36:178–183.

Polikanov YS, Melnikov SV, Söll D, Steitz TA. Structural insights into the role of rRNA modifications in protein synthesis and ribosome assembly. Nat. Struc. Mol. Biol. 2015; 22:342–344.

Rabl J, Leibundgut M, Ataide SF, Haag A, Ban N. Crystal structure of the eukaryotic 40S ribosomal subunit in complex with initiation factor 1. Science. 2011; 331:730–736. [PubMed: 21205638]

Scheres SH. RELION: implementation of a Bayesian approach to cryo-EM structure determination. J. Struct. Biol. 2012; 180:519–530. [PubMed: 23000701]

Schmeing TM, Huang KS, Kitchen DE, Strobel SA, Steitz TA. Structural insights into the roles of water and 2' hydroxyl of the P site tRNA in the peptidyl transferase reaction. Mol. Cell. 2005; 20:437–448. [PubMed: 16285925]

Schmidt C, Becker T, Heuer A, Braunger K, Shanmuganathan V, Pech M, Berninghausen O, Wilson DN, Beckmann R. Structure of the hypusinylated eukaryotic translation factor eIF-5A bound to the ribosome. Nuc. Acid Res. 2016; 44:1944–1951.

Strunk BS, Loucks CR, Su M, Vashisth H, Cheng S, Schilling J, Brooks CL, Karbstein K, Skiniotis G. Ribosome assembly factors prevent premature translation initiation by 40S assembly intermediates. Science. 2011; 333:1449–1453. [PubMed: 21835981]

Vincent Yip WS, Vincent NG, Baserga SJ. Ribonucleoproteins in Archaeal Pre-rRNA Processing and Modification. Archaea. 2013; 2013. doi: 10.1155/2013/614735

Wong W, Bai XC, Brown A, Fernandez IS, Hanssen E, Condron M, Tan YH, Baum J, Scheres SH. Cryo-EM structure of the Plasmodium falciparum 80S ribosome bound to the anti-protozoan drug emetine. eLife. 2014; 3:e03080.

Woolford JL, Baserga SJ. Ribosome Biogenesis in the Yeast Saccharomyces cerevisiae. Genetics. 2013; 195:643–81. [PubMed: 24190922]

Highlights

- 2.8-Å cryo-EM map of *Leishmania* ribosome facilitates atomic resolution structure.
- Direct observation of eukaryotic rRNA modifications.
- Leishmanial rRNA is fragmented and hyper modified at unique positions.
- Fragmented rRNA termini converge into three focal points involving 5.8S.

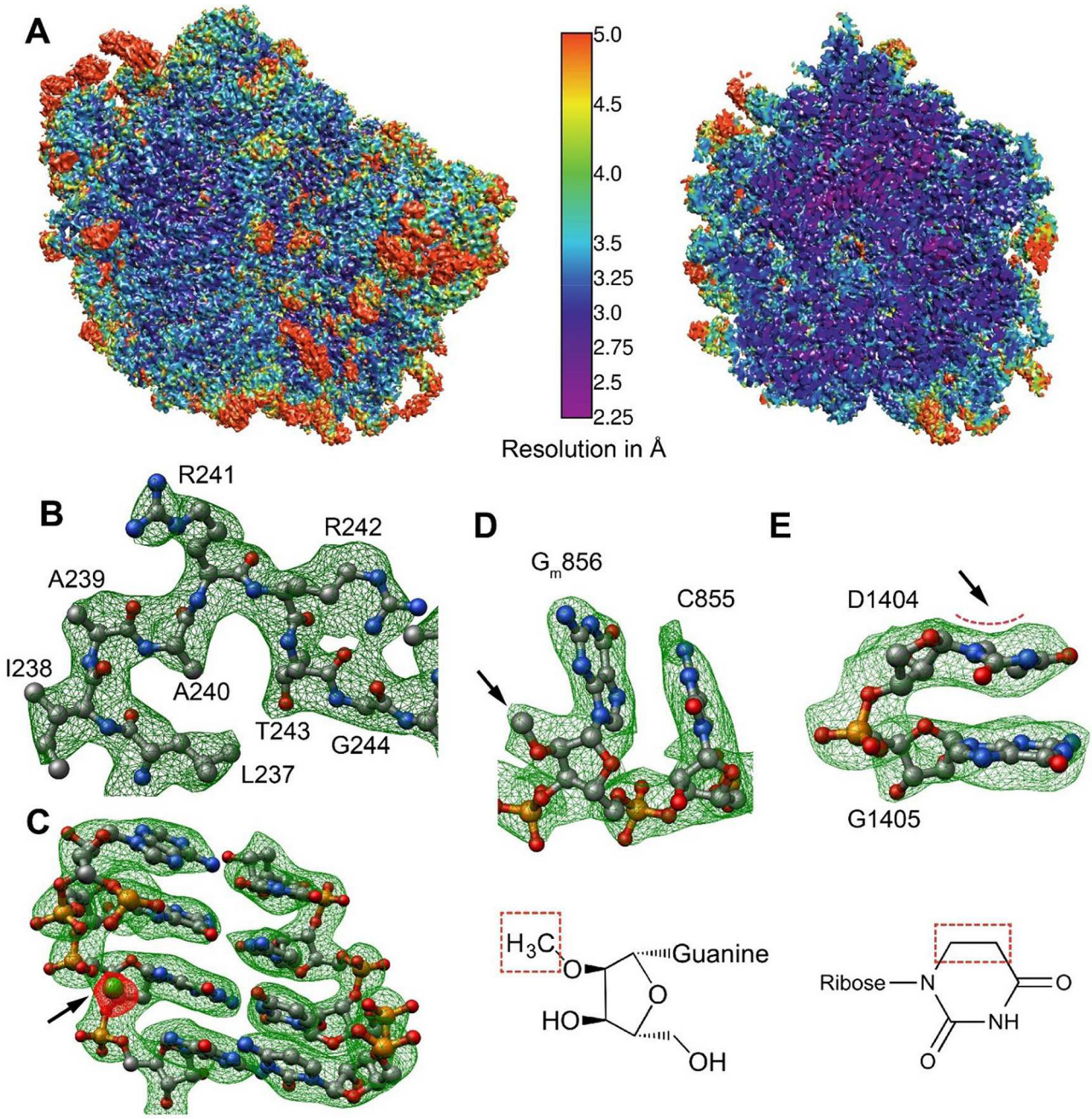

Figure 1. Cryo-EM map and modeling of *L. donovani* LSU

(A) Surface (left) and cross-section (right) representations of the cryo-EM density map colored according to local resolution distribution. **(B–C)** Snapshots of map *vs.* model from segments of protein uL2 **(B)** and 26S rRNA chain alpha **(C)**. The arrow in (C) points to the density (red) corresponding to a Mg^{+2} ion (green) interacting with the rRNA phosphate backbone. **(D–E)** Two examples of rRNA modifications observed. **(D)** The 2'-O methyl group of G856 of alpha 26S rRNA. A total of 46 2'-O methylated residues were modeled in the map. A detailed list of rRNA modifications is supplemented to the manuscript (Table

S4). **(E)** Dihydrouridine distorted ring in 26S rRNA residue U1404 of beta 26S. The arrows in (D) and (E) point to the densities for methyl group and ring distortion, respectively.

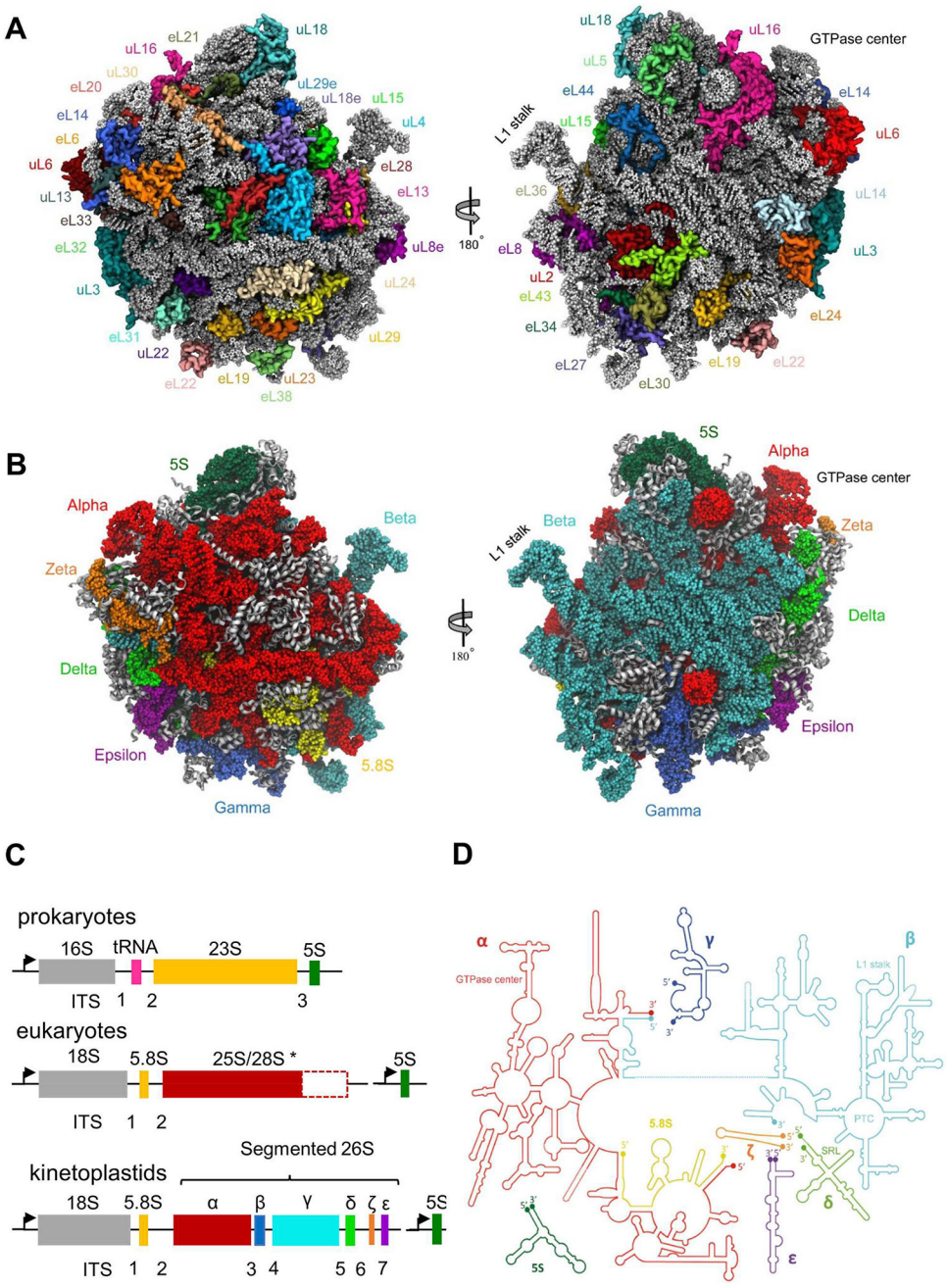

Figure 2. Structure of *L. donovani* LSU

(A) Protein distribution from two LSU views: solvent facing side (left) and subunit interface (right). Ribosomal proteins are shown as variably colored cartoon representations and rRNA as light grey ribbon. **(B)** Tertiary structure of rRNA distribution in the leishmanial ribosome LSU as viewed from either the solvent exposed side (left) or the inter-subunit interface (right). 5S rRNA is shown in dark green, 5.8S in yellow, and 26S rRNA segments α, β, γ, δ, ε and ζ are shown in red, cyan, blue, green, purple and orange, respectively. (**C**) Typical rRNA encoding operons in prokaryotes, eukaryotes and kinetoplastids. *The largest LSU component (25–28S) varies greatly in length within different species. In all panels,

promoters are marked as arrows pointing in the direction of transcription. Internal Transcribed Segments (ITSs) are numbered according to their order in the transcription unit. **(D)** Schematic diagram of rRNA secondary structure in *L. donovani* LSU. Functional sites are highlighted.

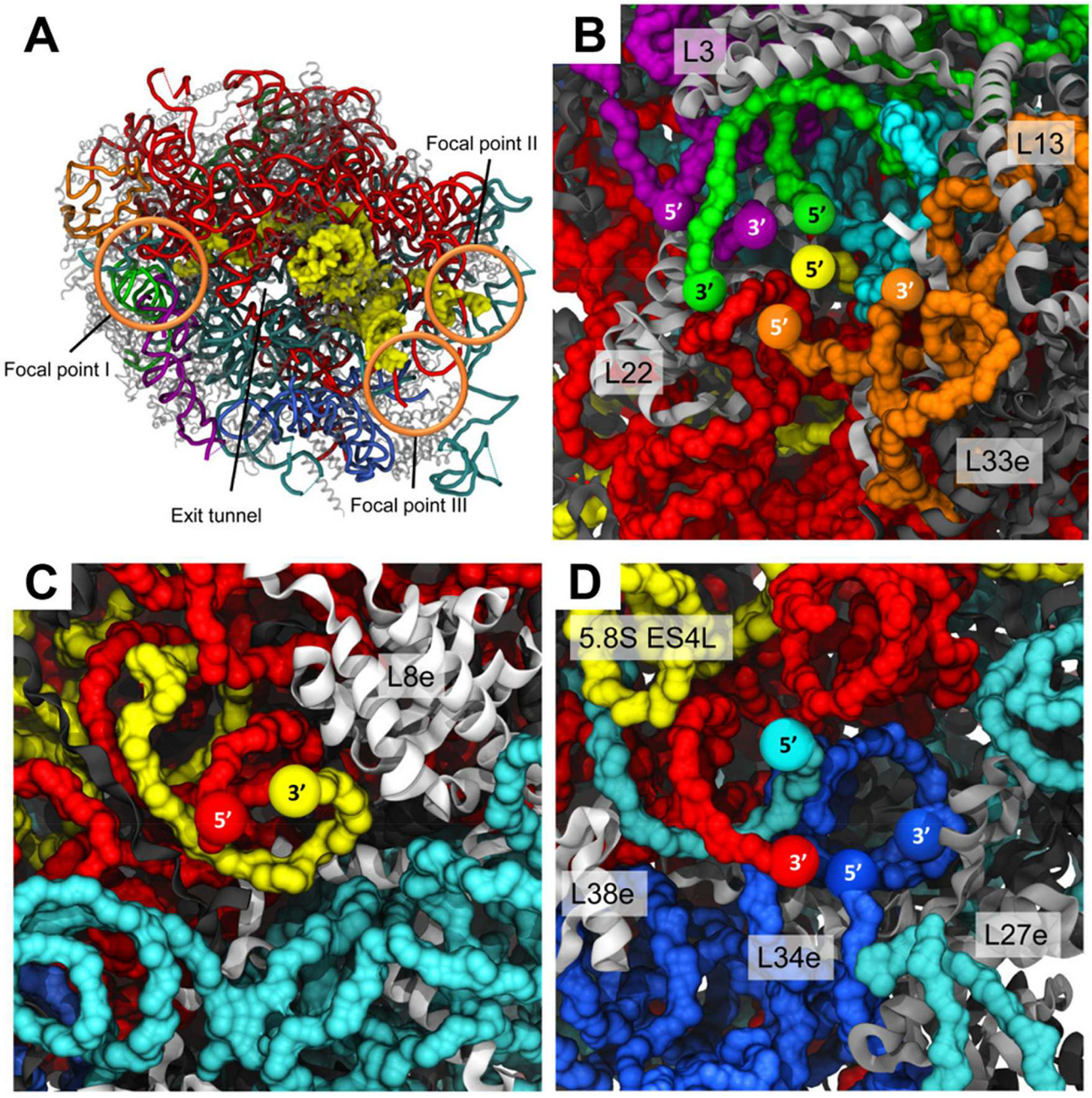

Figure 3. Focal points of LSU rRNA segmentation

26S rRNA segment terminals in the leishmanial ribosome converge to three focal points, all located on the solvent exposed side of the LSU. **(A)** LSU surface with localization of the three focal points in regards to the ribosome exit tunnel. The 5.8S rRNA chain is presented as yellow surface and all other chains are represented as cartoon tubes. **(B)** Focal point I includes the 5’ and 3’ ends of delta, epsilon and zeta, as well as the 5’ end of the 5.8S rRNA. **(C)** Focal point II includes alpha 5’ and 5.8S 3’ ends. **(D)** Focal point III includes both terminals of the gamma unit as well as alpha 3’ and beta 5’ ends. 5S rRNA is shown in dark green, 5.8S in yellow, and 26S segments α, β, γ, δ, ε and ζ are shown in red, cyan, blue,

green, purple and orange, respectively. Ribosomal proteins are illustrated as grey cartoons. Proteins in close proximity to the focal point cavity are labeled accordingly.

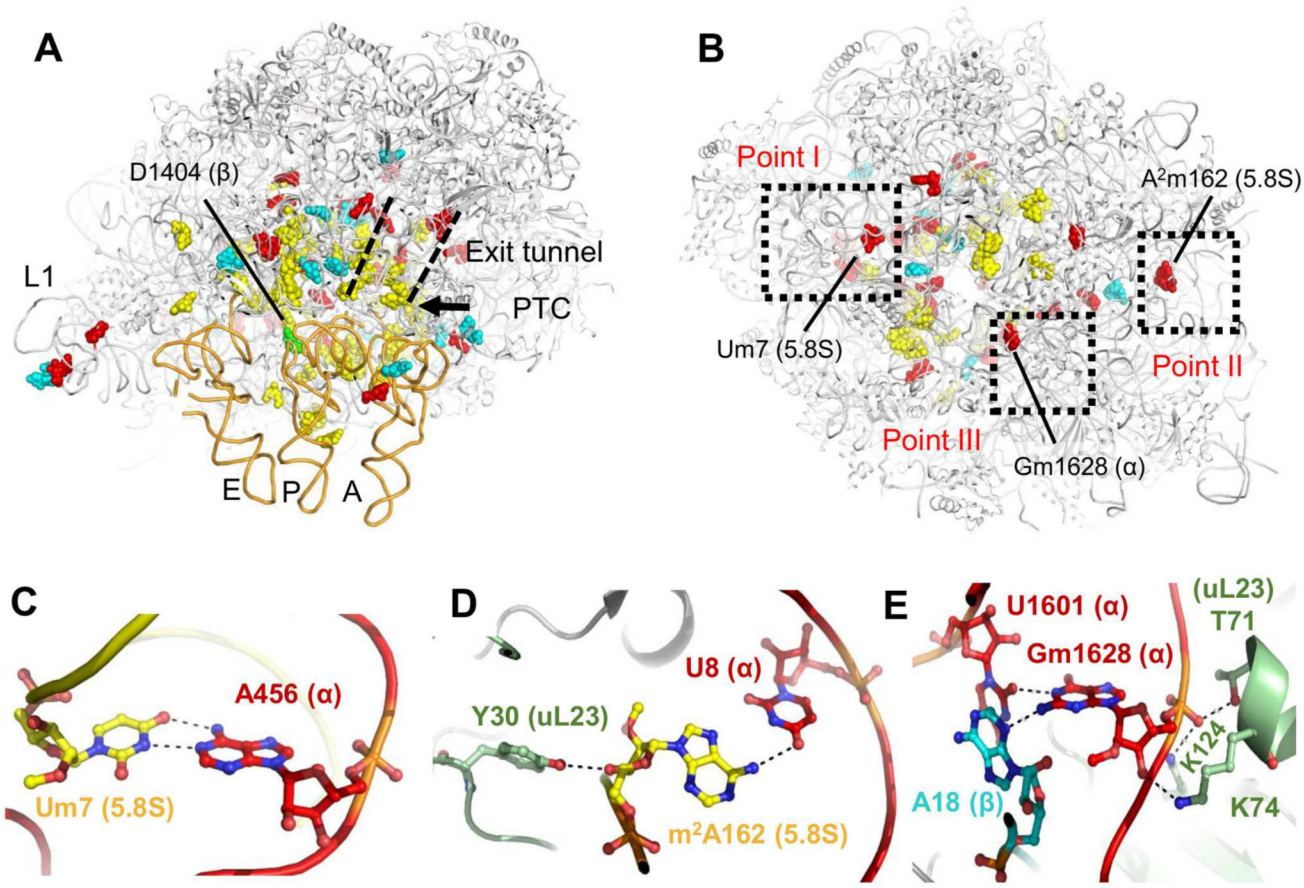

Figure 4. LSU rRNA modifications

Leishmania LSU rRNA is heavily modified by multiple 2'-O methyl groups and pseudouridins. Modified residues are mainly localized at functional ribosomal sites such as the PTC, the L1 stalk, the protein exit tunnel and all three tRNA binding sites (**A**) and are mostly distributed within internal parts of the ribosome (**B**). The predicted modified nucleotides as observed from two ribosomal views, one from the tRNA binding site in the subunit interface (**A**) and the other from the solvent exposed surface (**B**). 2'-O methylation sites that are unique to trypanosomatids are highlighted in red, pseudouridinylations in cyan and dihydrouridine in green. Eukaryote conserved residues are highlighted in yellow. A, P and E site-tRNAs are presented as orange tubes and were docked to their binding sites from previously reported yeast and rabbit cryo-EM structures of ribosomes at high resolution (Schmidt, et al., 2016; Brown, et al., 2015) Some rRNA modifications are also located in close proximity to the three focal points and interact with residues belonging to other chains. (**C–E**) Close up of modifications and their interaction networks in focal points I–III, respectively (also outlined in panel **B**). rRNA chains are colored in red, cyan, and yellow for alpha, beta, and 5.8S, respectively, and protein uL23 is shown in light green. Interacting residues are presented in a ball-and-stick representation and atoms are colored according to their identity. Polar contacts are presented as black dashed lines.